Kondo effect in a side-coupled double quantum dot system embedded in a mesoscopic ring

I-Ling Tsai[1] and Chung-Hou Chung[1,2]
[1]*Electrophysics Department, National Chiao-Tung University, HsinChu, Taiwan 300, Republic of China*
[2]*Departments of Physics and Applied Physics, Yale University, New Haven, Connecticut 06520, USA*
(Received 5 September 2009; revised manuscript received 2 February 2010; published 4 May 2010)

We study finite-size effect of the Kondo screening cloud in a double quantum dot setup via a large-N slave-boson mean-field theory. In this setup, one of the dots is embedded in a close metallic ring with a finite size L and the other dot is side coupled to the embedded dot via an antiferromagnetic spin-spin-exchange coupling with a strength K. The antiferromagnetic coupling favors local spin-singlet state and suppresses the Kondo screening. The mean-field phase diagram as a function of $1/L$ and K shows a crossover to the local spin-singlet ground state from the Kondo phase to occur at $K<K_c$ $(L=4n,4n+1,4n+3)$ and at $K>K_c$ $(L=4n+2)$. The effective Kondo temperature T_k (proptotional to inverse of the Kondo screening cloud size) shows the Kosterlitz-Thouless (KT) scaling at finite sizes for $L=4n,4n+2$, indicating quantum transition of the KT type between the Kondo screened phase for $K\leq K_c$ and a local spin-singlet phase for $K\geq K_c$ in the thermodynamic limit with K_c being the critical value. The local density of states on the embedded quantum dot and the persistent current at finite sizes with different values of K are calculated in the crossover region.

DOI: 10.1103/PhysRevB.81.195305 PACS number(s): 75.20.Hr

I. INTRODUCTION

The Kondo effect,[1] screening of magnetic impurities by conduction-electron reservoir, has been intensively studied over the last half century. Recently, there has been revived interest in Kondo effect in semiconductor quantum dot devices due to the progress in fabricating nanostructures.[3] When the number of electrons on the dot is odd, Kondo effect overcomes the Coulomb Blockade, leading to a narrow pronounced resonance peak in local impurity density of states and enhanced conductance through quantum dot devices.[2,3] Kondo effect is characterized by a single energy scale, the Kondo temperature $T_k \approx De^{-1/J}$,[1] below which the Kondo screening develops. Here, D, J in T_k are conduction-electron bandwidth and the dimensionless Kondo coupling, respectively. In a finite-sized mesoscopic device, T_k sets a length scale $\xi_k^0 \approx \hbar v_F/T_k$ associated with the size of the Kondo screening cloud where the cloud of electrons with a size of order of ξ_k^0 surrounding the magnetic impurity form spin-singlet state with it.[4] Here, v_F is the Fermi velocity. For typical values of T_k, ξ_k^0 is around $0.1-1$ μm, which is comparable to the typical size of quantum dot devices, leading to finite-size effects of the Kondo screening cloud. This effect has been investigated in a quantum dot embedded in a mesoscopic ring threaded by a magnetic field.[4–6] The experimentally measurable persistent current induced by a magnetic flux has been shown to be sensitive to the ratio of the size of the ring L and ξ_k^0.[4–6] As $L \ll \xi_K^0$ the Kondo screening cloud does not develop completely, giving rise to a suppression of Kondo effect and a reduction in the persistent current even if temperature is lower than T_k; while as for $L \gg \xi_k^0$ the Kondo screening cloud is already formed, leading to enhanced persistent current. By measuring transport properties (such as: persistent current) as a function of the system size, we gain insights on how the Kondo screening cloud is formed as the system size approaches to the thermodynamic limit. This idea offers another route to realize Wilson's numerical renormalization group (NRG) (Ref. 7) idea on the Kondo problem.

Very recently, study of the Kondo effect has been extended to coupled double quantum dot setups via antiferromagnetic (AF) Ruderman-Kittel-Kasuya-Yosida (RKKY) interactions.[8–11] Kondo effect in such double-dot systems competes with the RKKY interactions, giving rise to quantum phase transition in the context of the well-known two-impurity Kondo problem between the Kondo and local spin-singlet ground states.[13] Close to the quantum critical point, physical observables at finite temperatures exhibit non-Fermi-liquid behaviors. The crossover behaviors between these two phases can be accessed by changing temperatures. On the other hand, at zero temperature but at finite sizes, the size of the Kondo screening cloud provides us with an alternative route to the crossover behaviors in the two-impurity Kondo problem.[12]

In this paper, we study Kondo effect in a side-coupled double quantum dot system embedded in a finite-sized mesoscopic ring. A similar side-coupled double quantum dot system has been studied where one of the dots is coupled to Fermi-liquid leads of conduction electrons with a continuous spectrum.[14] Unlike the two-impurity Kondo system, in this side-coupled double-dot system the Kondo phase is fragile and unstable toward the local spin-singlet state for any infinite small antiferromagnetic spin-exchange coupling, and the transition is of the Kosterlitz-Thouless (KT) type. Note that a related setup consisting of double quantum dots in parallel connected to a mesoscopic ring shows a quantum phase transition of the pseudogap Anderson model when the magnetic flux is tuned.[15] Here, we are interested in not only the nature of the Kondo-to-spin-singlet quantum phase transition in our proposed setup but also the crossover properties via a systematic study of the system at finite sizes. The inverse of the system size $1/L$ plays a similar role as temperature T. At finite temperatures, crossover behaviors between these two quantum ground states can therefore be accessed effectively via changing the size of the ring.

We focus on the following three quantities to investigate this issue: the effective Kondo temperature T_k (inversely proportional to the size of the Kondo screening cloud ξ_k in the

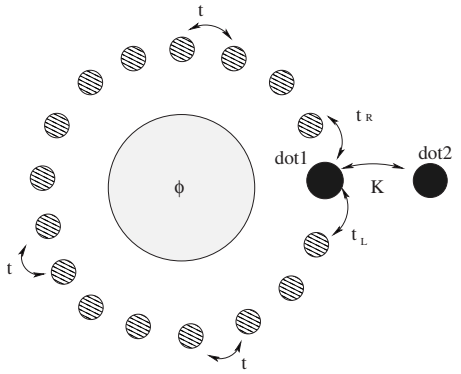

FIG. 1. Sketch of the model. t_L/t_R is the hopping coefficient between dot 1 and its left/right conducting island on the ring, ϕ is the magnetic flux (in unit of $2\pi/\Phi_0$ with $\Phi_0=hc/e$) through the ring, K is antiferromagnetic coupling between dot 1 and dot 2.

presence of the antiferromagnetic spin-exchange coupling), the local density of states (DOS) $\rho_{QD}(\omega)$ on the embedded quantum dot, and the persistent current (PC) I. The plan of the paper is as follows. In Sec. II., we introduce the model and present a large-N mean-field treatment of the model. In Sec. III., we present our results on the effective Kondo temperature, the local DOS on the dot, and the persistent current. We also give detailed explanations of our results. Conclusions are given in Sec. IV.

II. MODEL

Our model describes a double quantum dot system embedded in electronic reservoir in a finite-sized ring (see Fig. 1). In this setup, only one of the dots (dot 1) is coupled to the ring via hopping; while the other dot (dot 2) is coupled only to dot 1 via an antiferromagnetic spin-exchange interaction with the coupling strength K and is decoupled from the reservoir of the ring. The ring serves as electronic reservoir consists of $L-1$ conducting islands. We consider here the half-filled case ($N_e=L+1$ where N_e is the total number of electrons on the ring and on the two dots). The key point in this setup with a closed geometry is that the Kondo screening cloud is trapped in the ring and cannot escape into the external leads.[4] Nevertheless, one can measure the transmission probability through the quantum dot 1 embedded in the ring by measuring the persistent current[4,16] (see details in Sec. III.). Note that in an experimentally realistic setup, there exists direct hopping between the two quantum dots. However, strong Coulomb repulsion (or large charging energy) on the quantum dots strongly suppress the direct hopping. Nevertheless, an effective antiferromagnetic spin-spin-exchange coupling (RKKY coupling) is generated through the second-order hopping processes. A similar antiferromagnetic RKKY coupling has been argued to exist in an experiment of a coupled double quantum dot system via a third conduction-electron island in between the two dots.[8] To simplify our model, we restrict ourselves to only consider the antiferromagnetic spin-exchange coupling between the two quantum dots and neglect the direct hopping between the two dots. Our simplification can be justified in the strong Coulomb blockade regime where charging energy is very large and single occupancy on each dot is expected.[9,11]

The Hamiltonian of our model is given by

$$H = H_A + KS_1 \cdot S_2 \tag{1}$$

where H_A represents a quantum dot embedded in a ring by the Anderson impurity model,

$$H_A = -t\sum_{j=1}^{L-1}\sum_{\sigma}[c_j^\dagger c_{j+1} + \text{H.c.}] + U\sum_{i=1,2} n_{d_i}^{\uparrow} n_{d_i}^{\downarrow} + \sum_{\sigma,i=1,2} \epsilon_d d_{i\sigma}^\dagger d_{i\sigma} - \sum_{\sigma}[t_L d_{1\sigma}^\dagger c_{1\sigma} + t_R \exp(i\phi) c_{L-1\sigma}^\dagger d_{1\sigma} + \text{H.c.}] \tag{2}$$

where c_j, d_1, and d_2 represent the annihilation operators of electron on site j of the ring, dot 1 and dot 2, respectively, U is the on-site Coulomb repulsion (or charging energy) of the quantum dot, the phase factor ϕ is defined by $\phi=2\pi\Phi/\Phi_0$ with Φ being the magnetic flux going through the ring and $\Phi_0=hc/e$ being the flux quantum, t is the hopping of electrons within the tight-binding ring, and $t_{L/R}$ are the hopping between dot 1 and the two neighboring ring electrons c_{L-1}/c_1. Here, S_1 and S_2 represent spin operators of dot 1 and dot 2, respectively, with $S_i=\Sigma_{\sigma\sigma'} d_{i\sigma}^\dagger \sigma_{\sigma\sigma'} d_{i\sigma'}$. L is the total number of electrons in the system excluding dot 2. The well-known Kondo limit is reached for $U \gg t$ where due to large charging energy the single occupancy on each dot is expected: $n_{d1(2)} \approx 1$. Here, we consider a simple limit in the Kondo regime, $U \to \infty$ where the slave-boson mean-field (SBMF) approach[5,6] is applicable to simplify the quartic U term. Note that as a result of second-order hopping processes between the two dots, the strength of the antiferromagnetic exchange coupling behaves as $K \propto t_{12}^2/U$ with t_{12} being the hopping between dots 1 and 2. Nevertheless, as mentioned above, the direct hopping t_{12} term is strongly suppressed in the Kondo regime due to the single occupancy on each dot. We therefore drop the direct doping term in the following for simplicity.

Further progress can be made by decoupling the quartic spin-spin interaction $S_1 \cdot S_2$ into quadratic one via the Hubbard-Stratonovish transformation in the framework of the large-N $SU(N)$ mean-field theory where the symmetry of the Hamiltonian is generalized from the $SU(2)$ with spin degeneracy being two to $SU(N)$ with spin degeneracy being $N \to \infty$.[1,17] In the $SU(N)$ generalization of the slave-boson representation, the electron operators on the dots are given by: $d_{i\alpha}=f_{i\alpha} b_i^\dagger$ where the indices $\alpha=1,2,\ldots N$ and $i=1,2$ represent N flavors of the spin and the two quantum dots, respectively. The local constraints to enforce single occupancy on dots 1 and 2 are given by

$$\sum_{\alpha} f_i^{\dagger\alpha} f_{i\alpha} + b_i^\dagger b_i = \frac{N}{2}. \tag{3}$$

The mean-field Hamiltonian for H_A is therefore given by

$$NH_{A,MF} = -t\sum_{j=1}^{L-1}\sum_{\alpha=1}^{N}[c_{j\alpha}^{\dagger}c_{j+1\alpha} + \text{H.c.}] + \sum_{\alpha=1}^{N}\tilde{\epsilon}_d f_{1\alpha}^{\dagger}f_{1\alpha} + \sum_{\alpha=1}^{N}\epsilon_d' f_{2\alpha}^{\dagger}f_{2\alpha} - \sum_{\alpha=1}^{N}[\tilde{t}_L f_{1\alpha}^{\dagger}c_{1\alpha} + \tilde{t}_R \exp(i\phi)c_{L-1\alpha}^{\dagger}f_{1\alpha} + \text{H.c.}] + \lambda(b_0^2 - 1) + \bar{\lambda}(\bar{b}^2 - 1) \quad (4)$$

where $\tilde{t}_{L/R}=b_0 t_{L/R}$ with b_0 being the expectation value of the b_1 boson on dot 1, $b_0=\langle b_1\rangle$, $\bar{b}=\langle b_2\rangle$, $\lambda(\bar{\lambda})$ is the Lagrange multiplier which enforces local constraint Eq. (3) on dot 1 (2), $\tilde{\epsilon}_d=\epsilon_d-\lambda$, $\epsilon_d'=\epsilon_d-\bar{\lambda}$. The quartic antiferromagnetic spin-spin interaction can be decoupled via the mean-field variable χ,[17]

$$\chi = \frac{K}{N}\langle f_1^{\dagger\alpha} f_{2,\alpha}\rangle. \quad (5)$$

. Therefore, in the large-N limit,

$$\frac{K}{N}S_1\cdot S_2 = -\sum_{\alpha=1}^{N}\frac{\chi}{N}f_1^{\dagger\alpha}f_{2\alpha} + \text{H.c.} + \frac{\chi^2}{K}. \quad (6)$$

The full mean-field Hamiltonian is given by

$$H_{MF} = H_{A,MF} - \sum_{\alpha=1}^{N}\frac{\chi}{N}f_1^{\dagger\alpha}f_{2\alpha} + \text{H.c.} + \frac{\chi^2}{K}. \quad (7)$$

The mean-field energy E_{MF} can be obtained by diagonalizing the above Hamiltonian and it gives

$$E_{MF} = \sum_{m,\sigma}\epsilon_{m,\sigma}(\lambda, b_0) + \frac{\chi^2}{K} + \lambda(b_0^2 - 1) + \bar{\lambda}(\bar{b}^2 - 1), \quad (8)$$

where $\epsilon_{m,\sigma}$ are eigenvalues of the Hamiltonian matrix in H_{MF}, the summation over m includes all occupied levels of H_{MF}. Values of the mean-field variables λ, b_0, and χ are determined by minimizing E_{MF} with respect to b_0 and χ,

$$\frac{\partial E_{MF}}{\partial b_0} = \frac{\partial E_{MF}}{\partial \bar{b}} = \frac{\partial E_{MF}}{\partial \chi} = 0, \quad (9)$$

subject to the constraint equation $\partial E_{MF}/\partial\lambda = \partial E_{MF}/\partial\bar{\lambda} = 0$. The ground-state energy E_{gs} corresponds to the global minimum of $E_{MF}(\lambda, \bar{\lambda}, b_0, \bar{b}, \chi)$ which satisfies the mean-field equations. Note that the advantages of taking the large-N mean-field approach are: (i) in the large-N limit the solutions from the mean-field equations are exact though the physical system corresponds to $N=2$, and (ii) at finite N, a systematic $1/N$ correction to the mean-field results is possible though it is beyond the scope of this paper. The mean-field phase diagram can be mapped out via the solutions of the above mean-field equations.

III. RESULTS

Three physical observables are identified to investigate the Kondo screening effect of our setup at finite sizes: (i) *effective Kondo temperature* (T_k), (ii) *local density of states (LDOS) on dot 1* ($\rho_{QD}(\omega)$), and (iii) *PC*. Details are shown below.

Before we present our results, it is useful to summarize the behavior of the model at $K=0$ (without antiferromagnetic spin-spin coupling), which has been intensively studied in Refs. 4–6. The Kondo resonance of a quantum dot embedded in a mesoscopic ring strongly depends on the finite size L (mod 4), and the magnetic flux ϕ threading the ring. In particular, both the Kondo temperature T_k and the persistent current I follow universal scaling functions of ξ_k^0/L at a fixed magnetic flux. In the Kondo regime, all physical observables, such as: Kondo temperature T_k, persistent current I are enhanced as the size L increases but with different crossover behaviors in all four cases of $L=4n$, $L=4n+1$, $L=4n+2$, and $L=4n+3$. The magnetic-flux dependence of persistent current I exhibits a symmetry between size L and $L+2$: $I_L(\phi)=I_{L+2}(\phi+\pi)$, indicating that adding the magnetic flux of $\Phi_0/2$ (or adding a phase π) is equivalent to switch the behavior of the PC from a system with size L to $L+2$.

With the previous results in mind, we may discuss the general properties of our setup for $K>0$. Due to the antiferromagnetic spin-spin coupling, we expect in this case a competition between the Kondo and the local spin-singlet ground states, leading to the quantum phase transition. In fact, quantum phase transitions in double quantum dot systems with antiferromagnetic RKKY interactions have been intensively studied in recent years[8,9] in the framework of two-impurity Kondo problem[13] where the quantum dots couple to a conduction-electron Fermi sea with continuous spectrum. Two types of quantum phase transitions have been identified in these systems: the phase transition with a quantum critical point (QCP) and the one of the KT type. The characteristic behavior near QCP is the observables power-law dependence on the coupling strength relative to the critical point; while for the KT transition the crossover energy scale exponentially depend on the distance to the critical point. The former (QCP) type of the quantum phase transition is realized in the double-dot systems where each of the dot couples to an independent conduction-electron reservoir,[8,9] and the critical point separating the Kondo from the local spin-singlet phase is the well-known two-impurity Kondo fixed point.[13] The latter (KT) type exists in a side-coupled double-dot system where only one of the dots coupled to the electron reservoir.[14] The Kondo resonance becomes more fragile in the side-coupled system so that an infinite small antiferromagnetic coupling is sufficient to suppress the Kondo effect and leads to the spin-singlet ground state. We expect the similar Kosterlitz-Thouless transition to occur in our side-coupled double-dot system embedded in a ring. However, the mesoscopic ring in our setup consists of a finite number of tight-binding electrons (instead of a Fermi sea with continuous spectrum), the details of the transition might be different from those in Ref. 14 (see below).

A. Mean-field phase diagram

After solving the mean-field equations, we summarize our main results in the schematic mean-field phase diagram as shown in Fig. 2. We find the transition between the Kondo

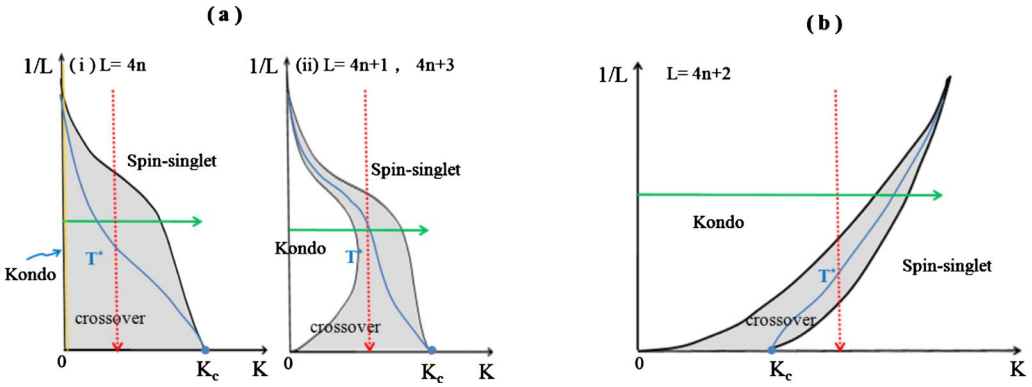

FIG. 2. (Color online) Schematic mean-field phase diagram of the model for (a) (i) $L=4n$ and (ii) $4n+1,4n+3$ [case (i)] and (b) $L=4n+2$ [case (II)]. The red (dark gray) dotted line with arrow indicates the crossover with K being fixed and the green (dark gray) solid line with arrow indicates the crossover with L being fixed. The crossover scales T^* in various cases are indicated by the blue (dark gray) solid lines. The Kondo phase in (a) (i) ($L=4n$) is indicated by the yellow (light gray) line along the vertical axis.

and spin-singlet phases is indeed of the Kosterlitz-Thouless type (see below). However, the K-T transition point K_c separating the two phases is not at zero as shown in the similar side-coupled double-dot system studied previously in Ref. 14 but at a finite value: $K=K_c>0$.

There are three regions in the phase diagram, corresponding to different mean-field solutions:

(1) for small K we find $b_0\neq 0$, $\lambda\neq 0$, and $\chi=0$. In the thermodynamic limit, this is the Kondo phase studied in Refs. 4–6.

(2) For large K, we find $b_0=0$, $\chi\neq 0$, and $\lambda\neq 0$. The ground state for $L\to\infty$ is the local spin-singlet phase where antiferromagnetic spin-spin coupling completely suppresses the Kondo effect.

(3) In the intermediate values of K, we find $b_0\neq 0$, $\lambda\neq 0$, and $\chi\neq 0$. This corresponds to the crossover region between Kondo and spin-singlet phases indicated in the shaded region in Fig. 2. This region is defined either by $K_{c1}<K<K_{c2}$ for a fixed size L where K_{c1} and K_{c2} are the boundaries between the crossover region and the two stable phases (the Kondo phase for K_{c1} and spin-singlet phase for K_{c2}) or by $L_{c1}<L<L_{c2}$ for a fixed K where L_{c1} and L_{c2} are defined in a similar way as K_{c1} and K_{c2}.

Note that in all the above three ranges in K values, we find $\bar{b}=0$, $\bar{\lambda}=\epsilon_d$. We now systematically investigate the crossover behaviors along the following two main different crossover paths, depending on the finite size L (mod 4).

Case (I) [Fig. 2(a)]: (i) for $L=4n$, and (ii) for $L=4n+1,4n+3$. We find these systems at finite sizes crossover from Kondo-to-spin-singlet ground state at K_{c2}, smaller than that in the thermodynamic limit K_c ($K_{c2}<K_c$). There are, however, differences in case (I) regarding the nature of the crossover region between even and odd sizes. For $L=4n$, we find $K_{c1}=0$, indicating a full crossover range $0<K<K_{c2}$; while for $L=4n+1,4n+3$, we find $K_{c1}>0$ and the crossovers at K_{c1} are of first-order level-crossing type. Though the values of K_{c1} increase slightly with increasing sizes for small sizes, at sufficiently large system sizes, however, further evidences (see below) indicate that in the limit of $L\to\infty$, K_{c1} is expected to vanish asymptotically, and the first-order transition at K_{c1} is expected to disappear.

Case (II) [Fig. 2(b)] occurs for $L=4n+2$ where we always find $K_{c2}>K_c$ at finite sizes though the crossover region may extend to $K<K_c$. At $K=K_{c1}$, we find that observables show a singular "kinklike" behavior. Nevertheless, as in the cases for $L=4n+1,4n+3$, the value of K_{c1} here also vanishes asymptotically in the limit of $L\to\infty$ (see below).

For $L=4n$ in case (I) and $L=4n+2$ in case (II), we find the crossover energy scale T^* follows the behavior of the typical Kosterlitz-Thouless transition in the crossover region, $K_{c1}<K<K_{c2}$,

$$T^* = c\widetilde{T}_k \exp[-\pi\widetilde{T}_k/(K-K_c)] \tag{10}$$

where $\widetilde{T}_k=c'T_k$, and both c and c' are nonuniversal constants.

We investigate the Kondo effect in our setup at finite sizes by either changing the size L at a fixed K [or following the red (vertical) dotted line with arrow in Fig. 2] or changing K at a fixed size L [or following the green (horizontal) solid line with arrow in Fig. 2]. The behavior of T_k vs K at finite sizes and finite-size scaling of T_k indicate that in the thermodynamic limit $L\to\infty$, $K_{c1}\to 0$; while K_{c2} converges to K_c, the K-T transition point: $K_{c2}\to K_c$ (see below).

B. Effective Kondo temperature

In the single Kondo dot system embedded in a two-dimensional electron gas, it is well known that the physical properties follow universal functions of (T/T_K^0) in Kondo regime where T_k^0 is the Kondo temperature of the single dot in the thermodynamic limit.[3] In a single quantum dot embedded in a mesoscopic ring with a finite size, the effective Kondo temperature can be defined as[5]

$$T_k^{1QD} = \epsilon_d - (E_{gs} - E_{gs}^o), \tag{11}$$

where ϵ_d is the energy of dot 1, E_{gs} and E_{gs}^0 correspond to the energy of the full system and of the tight-binding ring with the open boundary condition, respectively. The effective Kondo temperature T_k is the energy gain due to the coupling between quantum dot and the ring, which corresponds to the energy associated with the Kondo coupling. In the thermo-

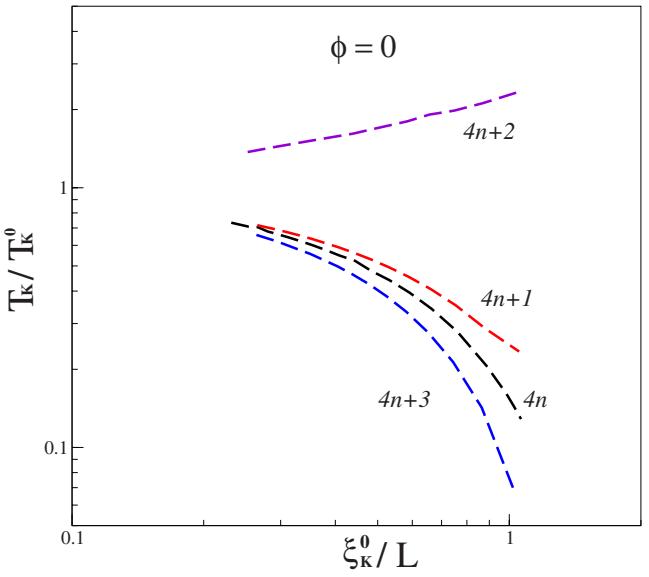

FIG. 3. (Color online) T_k at $K=0$ as functions of ξ_k^0/L. Parameters: $\epsilon_d=-0.8t$, $t_R=t_L=0.4t$, and $\phi=0$. Here we set $t=1$ as the unit.

dynamic limit ($L\to\infty$), T_k approaches to T_k^0. For relevant parameters in the $K=0$ Anderson model of the single dot-ring setup: $t=1$, $t_L=t_R=0.4t$, $\epsilon_d=-0.8t$, we find $T_k^0 \approx 0.0189t$, $\xi_k^0 \sim 106$. Note that for simplicity, we set $t=1$ throughout the paper as our unit. As a consistency check, we present the finite-size scaling for T_k at $K=0$ and $\phi=0$ as shown in Fig. 3. We find T_k/T_k^0 is indeed an universal function of ξ_k^0/L as shown in Refs. 5 and 6.

In the presence of the antiferromagnetic spin-spin coupling, the effective Kondo temperature T_k at a finite size in the context of our large-N slave-boson mean-field approach can be generalized from Eq. (11) to

$$T_k = \epsilon_d - (E_{gs} - E_{gs}^o) - \frac{\chi^2}{K}. \tag{12}$$

Note that the effective T_k defined in Eq. (11) is somewhat different from that defined in Ref. 5 where T_k is measured relative to the highest occupied (HO) level defined as ϵ_F.[5,6] We have checked that T_k from Eq. (11) here correctly reduces to 0 when the hopping between ring and dot 1 are turned off as there is no Kondo effect in a system of disconnected ring and dot; while T_k defined in Refs. 5 and 6 does not vanish in this case in general as ϵ_F is not zero in all four kinds of finite sizes. Meanwhile, the qualitative behaviors of T_k at finite sizes we obtained here via Eqs. (11) and (12) are consistent with our general mean-field phase diagram. In particular, in case (I) ($L=4n,4n+1,4n+3$) where the crossovers to the spin-singlet phase from the Kondo phase always occur at $K_{c2}<K_c$, we find $T_k<T_k^0$; while in case (II) ($L=4n+2$) where crossover to the singlet phase always happens at $K_{c2}>K_c$, we find the opposite: $T_k>T_k^0$. This qualitative behavior can be understood as follows: The key ingredient of our system is the competition between Kondo effect and the local AF spin-spin coupling, leading to the suppression of Kondo effect as the strength of the local AF spin-spin coupling K is increased. The energy scale associated with the Kondo effect is T_k; while the value K is a measure of the antiferromagnetic coupling strength between the two dots. The phase transition (or crossover at finite sizes) occurs at a finite value of K_c (K_{c2} at a finite size) where these two energy scales are comparable to each other. Therefore, we may consider $K_{c2}(L)$ at finite sizes as a reasonable estimation for $T_k(L)$ at finite sizes. For the crossover in case (I) where crossover to the spin-singlet phase occurs at $K_{c2}<K_c$, T_k is expected to be smaller than T_k^0 as it requires a weaker RKKY coupling $K_{c2}<K_c$ to suppress the Kondo state. Similarly, in case (II) where crossover occurs at $K_{c2}>K_c$, T_k at finite sizes is expected to be larger than T_k^0 since it requires a larger value $K_{c2}>K_c$ to suppress the Kondo effect at finite sizes compared to that in $L\to\infty$ limit. We have also checked that our results of T_k for $K=0$ are consistent with the finite-size behaviors in E_{gs} and E_{gs}^0 via perturbation theory in Ref. 4.

In the Kondo phase, T_k reduces to the Kondo temperature for the single quantum dot embedded in a mesoscopic ring ($K=0$). When $L\to\infty$, T_k in the Kondo phase approaches to T_K^0. In the crossover between Kondo and the local singlet phases, T_k decreases with increasing K, and finally $T_k\to 0$ when the system is in the local singlet ground state where the Kondo effect is completely suppressed by the antiferromagnetic spin-spin coupling. We analyze below in details the crossover between the Kondo and the local spin-singlet ground states from the behaviors of the Kondo temperature.

1. Varies K with fixed L

We first monitor how the Kondo resonance is destroyed by varying the antiferromagnetic spin-spin coupling strength K at a fixed finite size L. Figure 4 shows T_k as a function of antiferromagnetic coupling strength K at various fixed sizes. In both cases (I) and (II), T_k vanishes as $K\to K_{c2}$, indicating the suppression of Kondo resonance by the antiferromagnetic spin-spin interaction. However, there are differences between these two cases in how T_k vanishes as K increases. In case (I) and $L=4n$, we find $K_{c1}=0$ for all finite sizes ($100<L<800$) we have investigated. The crossover region therefore extends to the full range: $0<K<K_{c2}$ where T_k varies continuously [see Fig. 4(a)]. In case (I) and for $L=4n+1,4n+3$, we find for $K<K_{c1}$, T_k stays at a constant with the same value as that for the pure Kondo phase (T_k at $K=0$), followed by a first-order transition at K_{c1}, then a continuous crossover to the spin-singlet phase for $K_{c1}<K<K_{c2}$ (see Figs. 4(c) and 4(d)]. In case (II) ($L=4n+2$), we also find that T_k first remains a constant over a range for $K<K_{c1}$. However, instead of a first-order transition, T_k evolves continuously with K but with a sudden change in slope in T_k vs K at $K=K_{c1}$. We find this singular behavior consistent more with a "kinklike" behavior than a first-order level-crossing jump [see Fig. 4(b)]. The local density of state (LDOS) also shows the same qualitative behavior (see Fig. 8 below).

The fact that $K_{c2}>K_c$ in case (II) and $K_{c2}<K_c$ in case (I) suggests that at the mean-field level the Kondo effect at a finite size seems more robust in case (II) ($L=4n+2$) than in case (I) ($L=4n,4n+1,4n+3$). This is consistent with our numerical results as T_k for $L=4n+2$ is found to have the largest value among L (mod 4) for a given size.

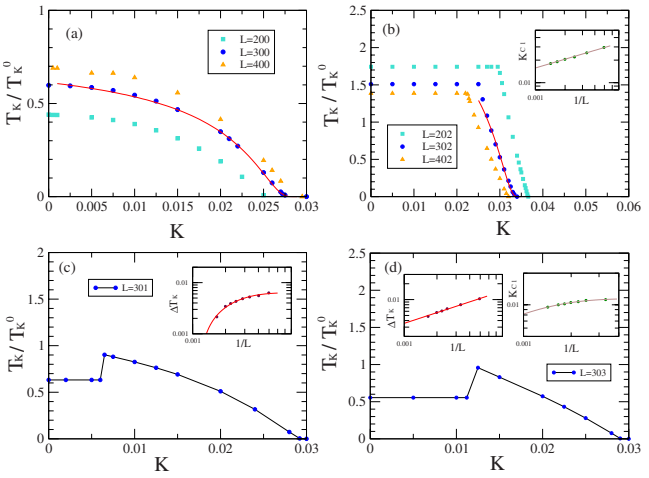

FIG. 4. (Color online) (a) T_k as functions of K for case I: $L=4n$ $(L=200,300,400)$ (b). T_k as functions of K for case II: $L=4n+2$ $(L=202,302,402)$. Inset in (b): K_{c1} as a function of $1/L$. Solid line is a fit to a power-law function of $1/L$. The solid lines in (a) and (b) are fits to the Kosterlitz-Thouless transition in Eq. (13) in the crossover region $K_{c1}<K<K_{c2}$. For $L=300$, $\alpha_1=0.01493$, $\alpha_2=0.00738$, $K_{c1}=0$, and $K_{c2}=0.029$. For $L=302$, $\alpha_1=0.057$, $\alpha_2=0.00845$, $K_{c1}=0.025$, and $K_{c2}=0.035$. (c). T_k as a function of K. for $L=4n+1$ $(L=301)$ [case (i)]. Inset: ΔT_k, the size of the first-order jump in T_k as a function of $1/L$ for $L=4n+1$ $(L=301)$. Solid line is a fit to an exponential function of $1/L$. (d) T_k as a function of K. for $L=4n+3$ $(L=303)$ [case (i)]. Inset (left): ΔT_k, the size of the first-order jump in T_k as a function of $1/L$ for $L=4n+3$. Solid line is a fit to a power-law function of $1/L$. Inset (right): K_{c1} as a function of $1/L$. Solid line is a fit to an exponential function of $1/L$. Other parameters: $\epsilon_d=-0.8t$, $t_R=t_L=0.4t$, and $\phi=0$. Here we set $t=1$ as the unit.

Note that at the general level these singular behaviors seen in various cases are likely due to the artifacts of the mean-field theory. They are expected to disappear in the thermodynamic limit or upon including fluctuations around the mean-field results.

To address the crossover behaviors for all four different sizes, we first focus on behavior of T_k vs K in the crossover region $K_{c1}<K<K_{c2}$ at finite sizes for $L=4n,4n+2$ where the physical observables evolve continuously. We find in the crossover region T_k vs K in both $L=4n$ and $L=4n+2$ can be fitted very well by the crossover of the Kosterlitz-Thouless type at finite sizes,

$$T_k = \alpha_1 \exp[-\alpha_2/|K-K_{c2}|] \tag{13}$$

where $\alpha_{1,2}$ are nonuniversal constants (see Fig. 4). Note that in the thermodynamic limit, $L\to\infty$, we have $K_{c2}\to K_c$. The above KT-type crossover form Eq. (13) reduces to the standard form $T_k=\alpha_1 \exp[-\alpha_2/|K-K_c|]$. The finite-size scaling (see below) of T_k also shows the same KT-type crossover behavior.

We now address the nature of the phase transitions in the thermodynamic limit. At a general level different behaviors at these four different sizes should merge in the thermodynamic (continuum) limit $L\to\infty$. For $L=4n$, we find that $K_{c1}=0$ and T_k vs K shows continuous Kosterlitz-Thouless type crossover behavior for all the finite sizes we investigated [see Fig. 4(a)]. It is therefore reasonable to expect that this behavior to survive in the thermodynamic limit, namely, T_k decreases continuously from T_k^0 (the Kondo temperature at $K=0$) to 0 upon increasing the RKKY coupling K from 0 to K_c. For $L=4n+2$, though T_k stays at a constant for $K\leq K_{c1}$, we find that the values of K_{c1} decrease in a power-law fashion with decreasing $1/L$ and that the crossover region of the KT type expands with increasing L [see Fig. 4(b)]. These behaviors suggest that in the thermodynamic limit $L\to\infty$, $K_{c1}\to 0$ and the full range $(0<K<K_c)$ of the Kosterlitz-Thouless crossover is expected, consistent with the behavior for $L=4n$.

For $L=4n+1,4n+3$, though the first-order transitions at K_{c1} are observed [see Figs. 4(c) and 4(d)], the jumps in T_k at $K=K_{c1}$, defined as ΔT_k, decrease (exponentially for $L=4n+1$ and in a power-law fashion for $L=4n+3$) with decreasing $1/L$ (see insets in Figs. 4(c) and 4(d)], indicating a weaker first-order transition at K_{c1} with increasing system sizes. Meanwhile, though for smaller system sizes we find K_{c1} increases with increasing sizes, for large system sizes, however, we find K_{c1} decreases exponentially with decreasing $1/L$ [see, for example, Fig. 2(a) and the inset in Fig. 4(d)]. We therefore expect that the first-order transitions seen for $L=4n+1,4n+3$ at finite sizes to disappear and $K_{c1}\to 0$ in the thermodynamic limit. Since on a general ground physical properties for all four different sizes should merge in the thermodynamic limit, it is reasonable to expect that the Kosterlitz-Thouless transition to occur for $L=4n+1,4n+3$ in the thermodynamic limit as well. However, to check this, we need to go to much larger system sizes $(L\geq 1000)$, which is beyond our numerical capability. We will therefore restrict ourselves to $L=4n,4n+2$ regarding the nature of the quantum phase transition in the thermodynamic limit.

2. Varies L with fixed K

Next, we present results on the finite-size dependence of the Kondo resonance at a fixed antiferromagnetic spin-spin coupling strength K. In analog to numerical renormalization group (NRG) method, the ground state is computed and monitored as we decrease the energy scale $1/L$ (or equivalently increase the system size L) until we reach the thermodynamic limit $L\to\infty$ (or effective zero temperature).

First, we describe qualitative behaviors of T_k at finite sizes in the two cases as mentioned above. For case (I) [$L=4n$, see Fig. 5(a)] T_k increases with increasing L and the Kondo resonance is recovered at large system size $L\gg\xi_k^0$ and with a reduced Kondo temperature T_k in the thermodynamic limit compared to that for $K=0$: $T_k<T_k^0$ for $L\to\infty$; while for case (II) [$L=4n+2$, see Fig. 5(b)] since crossover to the spin-singlet state occurs at $K_{c2}>K_c$, T_k decreases with increasing L and we expect that it vanishes in the thermodynamic limit: $T_k\to 0$ for $L\to\infty$. It is clear from the crossover behavior in Fig. 5 that the finite-size effect appears for $L<\xi_k^0$ where the Kondo screening cloud has not yet fully developed for $K<K_c$ and has not yet completely destroyed for $K>K_c$; while this effect diminishes as the system approaches to the thermodynamic limit or $L\gg\xi_k^0$. Note that in case (I) with large $K\gg K_c$ and case (II) with small $K\ll K_c$, the ground state re-

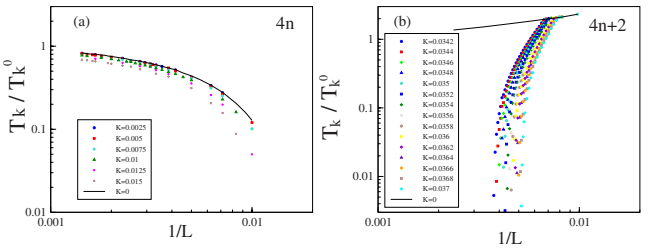

FIG. 5. (Color online) T_K as functions of $1/L$: (a) $L=4n$, K varies from $0.0025t$ to $0.015t$, distance: $0.0025t$. (b) $L=4n+2$, K varies from $0.036t$ to $0.04t$, distance: $0.001t$. Other parameters: $\epsilon_d=-0.8t$, $t_R=t_L=0.4t$, and $\phi=0$. Here, we set $t=1$ as the unit.

mains at local singlet and Kondo state, respectively; therefore, no crossover behaviors are found. Furthermore, T_k for $L=4n+2$ [case (II)] for $K=0$ approaches to T_k^0 from above as L approaches to the thermodynamic limit. This suggests that the Kondo effect in this case is more robust at finite size than in the thermodynamic limit. Therefore, at any finite size L, it is necessary to apply a larger antiferromagnetic coupling K compared to K_c which is required in $L\to\infty$ limit to suppress the Kondo effect. This provides an explanation on why we always find the crossover behavior for $L=4n+2$ for $K>K_c$. On the other hand in case (I) $(L=4n,4n+1,4n+3)$ for $K=0$, T_k approaches to T_k^0 from below as L increases, which explains why the crossover occurs for $K<K_c$ in this case.

To investigate the nature of the quantum phase transition in the thermodynamic limit more closely, we then perform the finite-size scaling for T_k in the crossover region. We find T_k in cases (I) $(L=4n)$ and (II) $(L=4n+2)$ follows its own unique universal scaling function of $1/(T^*L)$ as $K\to K_c$ (see Fig. 6), where T^* is the crossover energy scale defined as in Eq. (10): $T^*=c\widetilde{T}_k \exp(-\pi\widetilde{T}_k/|K-K_c|)$ with $\widetilde{T}_k=c'T_k$ has the same form in both cases (I) and (II) $(L=4n+2)$. Here, c, c', K_c are nonuniversal fitting prefactors depending on the initial parameters of the Hamiltonian. For $\epsilon_d=-0.8t$, $t_R=t_L=0.4t$, $\phi=0$, we find $c\approx 5.5$, $K_c\approx 0.0271$ (in unit of t) in both cases (I) and (II); $c'\approx 0.65$ in case (I), and $c'\approx 0.5$ for case (II). Note that the expression for T^* in Eq. (10) is quite general as K can be either smaller [case (I)] or larger [case (II)] than K_c. The universal scaling at finite sizes and the same exponential form for the crossover energy scale T^* valid for both cases indicate that in the thermodynamic limit the system exhibits the Kosterlitz-Thouless transition at a finite antiferromagnetic spin-spin coupling strength $K_c>0$. We have checked the consistency of our result from our finite-size scaling that K_c indeed reaches to the same value in the thermodynamic limit for both cases (I) and (II) even though the corresponding crossover regions we investigate are on the opposite side of the transition [$K<K_c$ for case (I) and $K>K_c$ for case (II)].

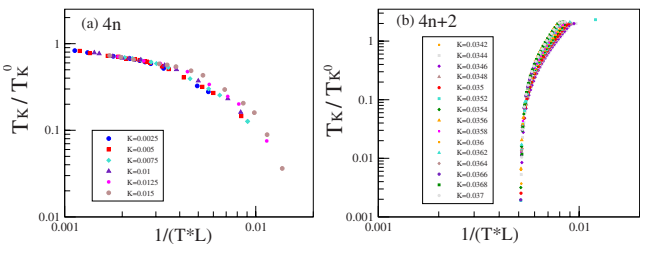

FIG. 6. (Color online) T_K as functions of $1/(T^*L)$: (a) $L=4n$, K varies from $0.0025t$ to $0.015t$, distance: $0.0025t$. (b) $L=4n+2$, K varies from $0.036t$ to $0.04t$, distance: $0.001t$. T_K follows universal scaling functions of $1/(T^*L)$. Other parameters: $\epsilon_d=-0.8t$, $t_R=t_L=0.4t$, and $\phi=0$. Here, we set $t=1$.

As a consistency check, for $L=4n$, as the system approaches to the thermodynamic limit, $L\to\infty$ and with increasing K, we find T_k reduces further its value from T_k^0: $T_k\to T_k(L=\infty)<T_k^0$ (see Fig. 5), which is consistent with behavior in T_k vs K [see Fig. 4(a)]. For $L=4n+2$, we find $T_k\to 0$, as expected (see Fig. 6).

Note that in spite of the singular behavior at K_{c1} (or L_{c1}) for $L=4n+2$, for large system sizes and K being sufficiently close to K_c, we find the finite-size scaling of T_k still follows the typical Kosterlitz-Thouless transition as that for $L=4n$ with the same level of quality [see Figs. 6(a) and 6(b)]. However, for smaller sizes and for K being further away from K_c, we find that the quality of the Kosterlitz-Thouless crossover behavior is reduced, which may be related to the singular behavior at K_{c1}. Nevertheless, for large system sizes and for K being sufficiently close to K_c, this singular behavior does not seem to affect the Kosterlitz-Thouless nature of the crossover behavior for $L=4n+2$. This is expected as in the thermodynamic limit the nature of the phase transition obtained from all four different sizes should agree.

Note that unlike the similar side-coupled double-dot system studied previously in Ref. 14 where the KT transition between the Kondo and spin-singlet phase occurs at $K_c=0$, we find in our setup a finite $K_c>0$ for the same KT transition. We think this difference might be related to the more singular DOS of the conduction-electron bath in the current setup of a tight-binding ring compared to that in a continuous Fermi sea with a constant DOS, making the Kondo resonance more robust against the antiferromagnetic spin-spin coupling in the current set up and therefore leads to a finite K_c instead of $K_c=0$. Further study is necessary to clarify this issue.

C. Local density of state

We now turn our attention to the LDOS on dot 1, given by

$$\rho_{QD}(\omega)=-\frac{1}{\pi}\mathrm{Im}\, G^R_{d_1d_1}(\omega) \tag{14}$$

where $G^R_{d_1d_1}(t)\equiv\langle d_1(t)d_1^\dagger(0)\rangle$ is the retarded Green's function of dot 1 which directly couples to the ring. Near the Fermi surface, $\rho_{QD}(\omega)$ determines the transport properties of the system, and it can be obtained from the Green's function $G_{d_1d_1}(\omega)$ via equation of motion approach. First, the mean-field Hamiltonian in momentum space is given by

$$H_{MF}=\sum_{m,\sigma}\epsilon_m c_m^\dagger c_m+\mathrm{H.c.}+\widetilde{\epsilon}_d f_{1\sigma}^\dagger f_{1\sigma}-\sum_m (t_m c_m^\dagger f_1+\mathrm{H.c.})$$
$$-\chi f_1^\dagger f_2-\mathrm{H.c.}+\frac{\chi^2}{K}+\lambda(b_0^2-1), \tag{15}$$

where

$$t_m = i\sqrt{\frac{2}{L}}\sin\left(\frac{m}{L}\pi\right)[\tilde{t}_L + \tilde{t}_R \exp(i\phi)(-1)^{m+1}] \quad (16)$$

with $m=1,2,\ldots L-1$.[5]

The equation for a general retarded Green's function $G^R_{ij}(\omega)$ is then given by

$$(\omega + i\eta - H_{MF})G^R_{ij}(\omega) = I \quad (17)$$

where I is the identity matrix, i,j can be f_1, f_2, or m. We therefore get the following three equations for $G_{f_1f_1}$, G_{f_1m}, and $G_{f_1f_2}$:

$$(\omega + i\eta - \tilde{\epsilon}_d)G^R_{f_1f_1}(\omega) - \chi G^R_{f_2f_1} - \sum_m t_m G^R_{md1}(\omega) = 1, \quad (18)$$

$$-\chi G^R_{f_1f_1} + (\omega + i\eta)G^R_{f_2f_1} = 0, \quad (19)$$

$$-t_m G^R_{f_1f_1} + (\omega + i\eta - \epsilon_m)G^R_{mf_1} = 0. \quad (20)$$

The above equations are easily solved and we get

$$G^R_{d_1d_1}(\omega) = b_0^2 G^R_{f_1f_1} = \frac{b_0^2}{\omega - \tilde{\epsilon}_d + i\eta - \sum_m \left[\frac{t_m^2|b_0|^2}{\omega - \epsilon_m + i\eta}\right] - \frac{\chi^2}{\omega + i\eta}} \quad (21)$$

where $\eta \to 0$. We then obtain $\rho_{QD}(\omega)$ by Eq. (14). In the following we analyze the crossover behaviors in LDOS $\rho_{QD}(\omega)$.

1. $K=0$

In the absence of the antiferromagnetic spin-spin coupling ($K=0$), the LDOS has been extensively studied where $\rho_{QD}(\omega)$ depends sensitively on L (mod 4) at finite sizes.[5] As shown in Fig. 7, our results on LDOS in this case at finite sizes are qualitatively in good agreement with that in Ref. 5. For the convenience of later discussions we summarize below the behaviors of LDOS in the four different cases of L. The key features are: (i) there exists a main Kondo resonance peak (located either symmetrically or asymmetrically with respect to $\omega=0$) followed by pairs of side peaks. (ii) As shown in Fig. 7, as L increases the main Kondo peak gets more pronounced and closer to $\omega=0$; while the side peaks are gradually merged into the broadened main peaks. In particular, the LDOS for $L=4n$ is very symmetric $\rho_{QD}(\omega) = \rho_{QD}(-\omega)$, suggesting the symmetry between particle and hole excitation energy in the finite-size spectrum. The asymmetric Kondo peaks for $L=4n+1$ and $L=4n+3$ are located on the opposite sides (left for $L=4n+1$ and right for $L=4n+3$) of ω. For $L=4n+2$, however, the LDOS shows asymmetric double Kondo peaks with comparable sizes and a dip at $\omega=0$. These differences in DOS among the four sizes of L (mod 4) can be explained in terms of the energy levels corresponding to the HO and the lowest unoccupied (LU) states relative to the Fermi level:[5] For $L=4n$, both HO and LU levels are around the Fermi energy $\epsilon_F=0$, leading to a symmetric single peak in LDOS at $\omega=0$. For $L=4n\pm1$, HO and LU levels are both below and above ϵ_F, respectively, giving rise to an asymmetric single peak in LDOS below and above $\omega=0$ separately. However, for $L=4n+2$, LU and HO levels are on the opposite side of the Fermi level with an unequal distance to the Fermi level, resulting in splitted asymmetrical double Kondo peaks below and above $\omega=0$. It should be noted that despite the differences at finite sizes ($L \sim \xi_k^0$), the LDOS in all four cases indeed merges to a single Kondo peak as the system reaches the thermodynamic limit $L \to \infty$ (or $L \gg \xi_k^0$). (iii) The LDOS on dot 1 obeys the following symmetries:[5] $\rho^L_{QD}(\omega,\phi) = \rho^{L+2}_{QD}(\omega,\phi+\pi)$ and $\rho_{QD}(-\omega,\phi) = \rho_{QD}(\omega,\phi+\pi)$.

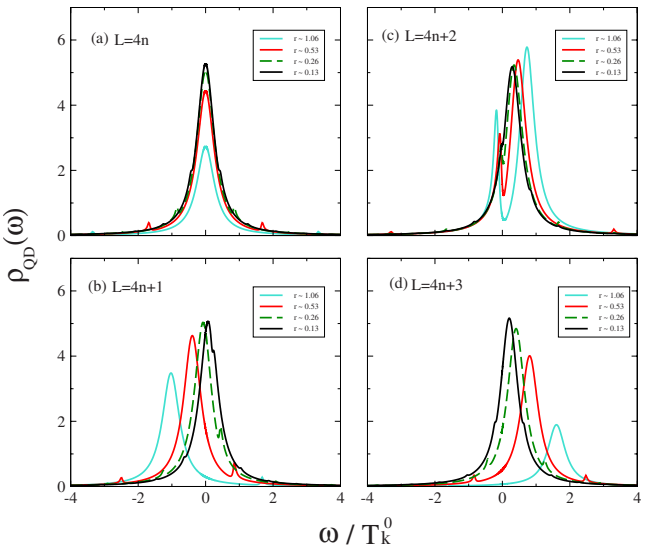

FIG. 7. (Color online) Local density of states for $K=0$ system (in arbitrary unit) (a) $L=4n$, (b) $L=4n+1$, (c) $L=4n+2$, (d) $L=4n+3$. Here, $r=\xi_k^0/L$, the ratio between ξ_k^0 and L. Other parameters: $\epsilon_d=-0.8t$, $t_R=t_L=0.4t$, and $\phi=0$. Here, we set $t=1$.

We would like to point out here that from the width D of the central Kondo peak(s), which can be approximately regarded as a quantity proportional to the effective Kondo temperature T_k, in LDOS for $K=0$ case one can qualitatively understand the opposite trends in T_k at finite sizes in cases (I) and (II) mentioned above. For $L=4n,4n+1,4n+3$ [case (I)], the width D becomes larger as L increases, indicating an increase in T_k as the system approaches to the thermodynamic limit; while as for $L=4n+2$ [case (II)], D gets smaller as L increases, suggesting a decrease in T_k as $L \to \infty$. We analyze in details below the behaviors of LDOS for $K>0$.

2. $K>0$

At a finite $K>0$, the LDOS on the dot shows a crossover between the Kondo phase and the spin-singlet phase. For $K<K_{c1}$ at a fixed size L, the LDOS remains the same as that for $K=0$. For $L=4n,4n+2$ we find a continuous evolution in LDOS from Kondo to the crossover region near $K=K_{c1}$ [see Figs. 8(a) and 8(c)]; while for $L=4n+1,4n+3$ the LDOS exhibits a first-order transition with a sudden shift of spectral weight at K_{c1} [see Figs. 8(b) and 8(d)]. Note that from Fig.

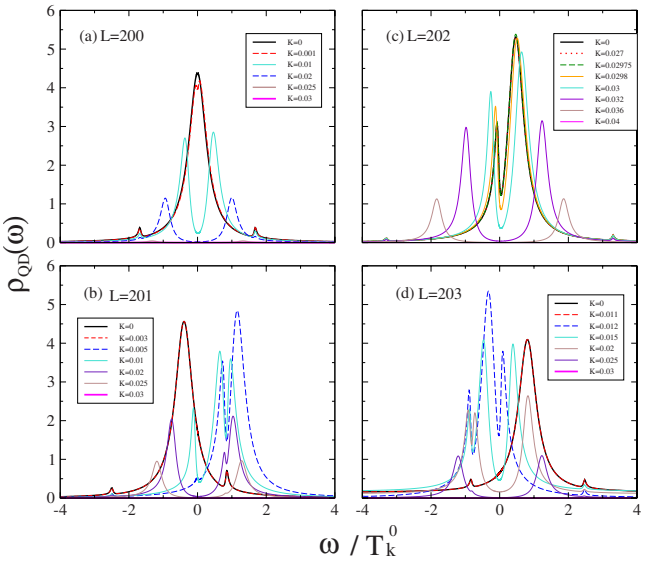

FIG. 8. (Color online) Local density of states (in arbitrary unit) with various K for $r=\xi_k^0/L\sim 0.53$. (a) $L=4n$, $K_{c1}=0$, and $K_{c2}=0.0288$. (b) $L=4n+1$, $K_{c1}=0.005$, and $K_{c2}=0.03$. (c) $L=4n+2$, $K_{c1}=0.02975$, and $K_{c2}=0.04$. (d) $L=4n+3$, $K_{c1}=0.012$, and $K_{c2}=0.03$. Other parameters: $\epsilon_d=-0.8t$, $t_R=t_L=0.4t$, and $\phi=0$. Here, K is in unit of t, and we set $t=1$.

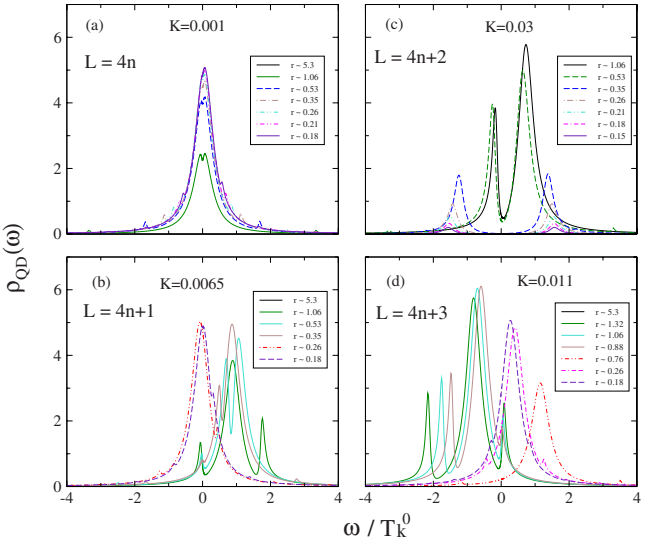

FIG. 9. (Color online) Local density of states (in arbitrary unit) with various L and fixed K (in unit of t). Here, $r=\xi_k^0/L$. (a) $L=4n$, (b) $L=4n+1$, (c) $L=4n+2$, (d) $L=4n+3$. Other parameters: $\epsilon_d=-0.8t$, $t_R=t_L=0.4t$, and $\phi=0$. Here, we set $t=1$.

8(c), LDOS for $L=4n+2$ is more consistent with a "kinklike" singular behavior than a first-order transition since LDOS does not change for $K<K_{c1}$, then followed by a continuous change in LDOS for $K\geq K_{c1}$ (see continuous evolution of LDOS for $K=0.0297, 0.02975, 0.0298, 0.03$). This is consistent with behaviors seen in Fig. 4(b). For $K>K_{c2}$, we find $\rho_{QD}(\omega)=0$ as an indicator of the local spin-singlet phase since $b_0=0$. In the crossover region $K_{c1}<K<K_{c2}$, the Kondo peak in LDOS splits into two with respective to $\omega=0$. The splitting gets wider as K increases further. Details are shown below.

a. Varies K with fixed L . In Fig. 8, we show LDOS for various antiferromagnetic spin-spin coupling strength K at a fixed size $L\approx 200(\xi_k^0/L\sim 0.5)$. Behaviors of LDOS are classified by L (mod 4). The common features in Fig. 8 are as follows. The Kondo peak in all four cases in $\rho_{QD}(\omega)$ splits into two at a small value of $K>K_{c1}$, indicating a crossover between Kondo and local spin-singlet phases. The two peaks in crossover region separate further apart and become more symmetric as K increases. At the end, $\rho_{QD}(\omega)$ vanishes when $K>K_{c2}$ in the local spin-singlet phase. Note that the values for K_{c2} depend sensitively on L (mod 4). This can be understood as when $L\approx 200$ the effective Kondo temperature T_k in case (II) is much larger than that in case (I) (see Figs. 5 and 6), which explains why a larger value of K_{c2} is needed in case (II) to suppress the Kondo effect than that in case (I). We present details below.

b. Varies L with fixed K . Figure 9 shows how $\rho_{QD}(\omega)$ changes with the system size L. For $0<K<K_c$, starting from a small size $L<L_{c1}$, the LDOS changes from the behavior of a local spin-singlet state with $\rho_{QD}(\omega)=0$ to that in the crossover region with splitted peaks and finite LDOS at $\omega=0$, and finally it recovers the Kondo resonance at larger size $L>L_{c2}$.

We separate discussions here into two different cases: $K<K_c$ [case (I)] and $K>K_c$ [case (II)]. Figures 9(a), 9(b), and 9(d) show finite-size dependence of $\rho_{QD}(\omega)$ at $K<K_c$ [case (I)] for $L=4n$, $4n+1$, and $4n+3$, respectively. For small system sizes, the system is in the local spin-singlet state with vanishing LDOS. At intermediate sizes in the crossover region, however, LDOS starts to develop peaks with a dip at $\omega=0$. As size further increases, these splitted peaks either gradually ($L=4n$) or suddenly ($L=4n+1$ and $4n+3$) merge into a single Kondo peak located either symmetrically ($L=4n$) or asymmetrically ($L=4n+1$ and $4n+3$) with respect to $\omega=0$. These Kondo peaks then follow the evolution at finite sizes for $K=0$ and finally recover the single symmetric Kondo peak in the thermodynamic limit.

For $K>K_c$ [case (II)], the size dependence of $\rho_{QD}(\omega)$ is shown in Fig. 9(c) with $K=0.03t>K_c$. The LDOS exhibits a crossover from the Kondo-to-local-spin-singlet state with increasing size L. For $K\sim K_c$ the LDOS changes from singlet state at small sizes to the crossover regime $100<L<800$ that we investigate. To study the ultimate fate of the system one needs to go much larger system size than $L\sim 800$, which is beyond the scope of our computational limit. Note that our analysis on the LDOS by changing K with fixed L (changing L with fixed K) is consistent with the horizontal green line (vertical red line) of the schematic phase diagram shown in Fig. 2. Finally, we believe the first-order transitions seen in LDOS at $K=K_{c1}$ for $L=4n+1$ and $L=4n+3$ are likely due to the artifact of the mean-field theory. Further investigation is needed to clarify this issue.

D. Persistent current

We now analyze the crossover from behaviors in persistent current. The Kondo screening cloud in our closed setup

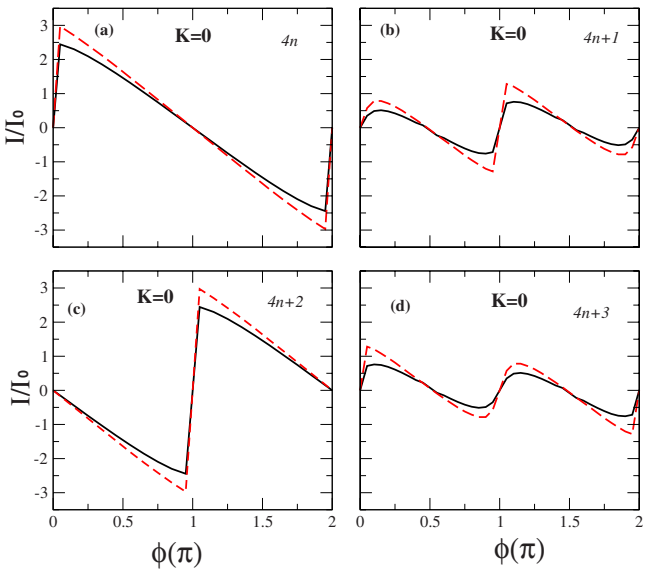

FIG. 10. (Color online) Persistent current (in unit of I_0) versus magnetic flux (in unit of $2\pi/\Phi_0$) with $K=0$. Red (dark gray) dashed line is for $r=\xi_k^0\sim 0.53$. Black solid line is for $\xi_k^0/L\sim 1.06$. (a) $L=4n$, (b) $L=4n+1$, (c) $L=4n+2$, and (d) $L=4n+3$. Other parameters: $\epsilon_d=-0.8t$, $t_R=t_L=0.4t$. Here, we set $t=1$.

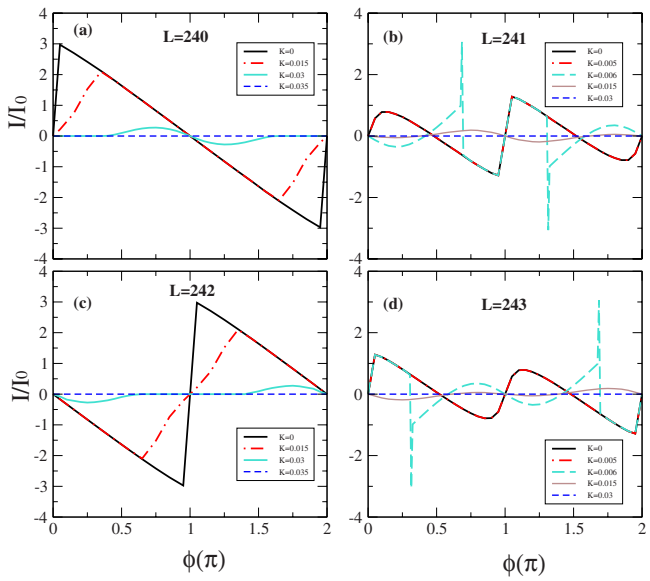

FIG. 11. (Color online) Persistent current versus ϕ with various K for $L\sim 240(\xi_k^0/L\sim 0.44)$. $K=0,0.015,0.03$ (in unit of t). (a) $L=4n$, (b) $L=4n+1$, (c) $L=4n+2$, and (d) $L=4n+3$. Other parameters of data: $\epsilon_d=-0.8t$, $t_R=t_L=0.4t$. Here, we set $t=1$. For $L=4n,4n+2$, $K_{c1}=0$, $K_{c2}=0.035$; while for $L=4n+1,4n+3$, $K_{c1}=0.005$, $K_{c2}=0.03$.

is restricted itself in the ring. To get an experimental access, one possible way is to measure persistent current (PC) induced by changing the magnetic flux threading the ring without attaching leads to it. PC is defined as

$$I=-\frac{e}{\hbar}\frac{\partial E_{gs}}{\partial \phi}. \tag{22}$$

PC can be served as a detector for the Kondo screening cloud since as a function of ϕ PC behaves very differently when $\xi_k \gg L$ than when $\xi_k \ll L$. Such persistent current experiments have been reported recently on micron sized ring without containing the dot.[18] In our setup, PC can be used to measure the strength of the Kondo correlation as the antiferromagnetic coupling K is expected to suppress the Kondo effect, leading to a weaker PC.

E. $K=0$

Before we present our results on the PC, it proves useful to summarize the previous results[4,5] for $K=0$. As shown in Fig. 10, since the system is in the Kondo regime, PC increases with increasing system size L. PC as a function of the magnetic flux is a weak sinusoidal wave when $L\ll\xi_k^0$; while it behaves like a sawtooth when $L\gg\xi_k^0$. Meanwhile, there exists a relation between PC for L and $L+2$: $I_N(\phi)=I_{N+2}(\phi+\pi)$ (Refs. 4 and 5) due to the π shift in LDOS of the quantum dot from the system with N sites to $N+2$ sites. Furthermore, the magnitude of PC for $L=$odd is much smaller than that for $L=$even. This can be understood as for $L=$odd the electrons are fully occupied at the Fermi level, which suppresses the Kondo resonance; while as for $L=$even there is an unpaired electron on the Fermi level, leading to the Kondo resonance. The results for $K>0$ are shown below.

1. Varies K with fixed L

PC (in unit of I_0 where $I_0=ev_F/L$ is the persistent current of an ideal metallic ring with v_F being Fermi velocity) versus magnetic flux with different antiferromagnetic coupling strength K at a finite size $L\sim 240(\xi_k^0/L\sim 0.44)$ is shown in Fig. 11. The general trend in all four cases is that the amplitude of PC gets smaller as K is increased and finally vanishes for $K>K_{c2}$, in agreement with our expectation on the suppression of the Kondo effect by the antiferromagnetic spin-spin coupling. Also, as shown in Fig. 11, the shape of the PC as a function of ϕ changes from sawtooth shape at smaller K values to weak sinusoidal waves at larger K values, similar to that for $K=0$. There are detailed differences among the four cases. In Figs. 11(a) and 11(c), with increasing K the persistent current $I_{L=240}$ near $0.5\pi<\phi<1.5\pi$ decreases more slowly than that for $0\pi<\phi<0.5\pi$ and $1.5\pi<\phi<2\pi$; similarly for $I_{L=242}$ except for the range of ϕ is being interchanged. This suggests that the Kondo effect is more robust in $0.5\pi<\phi<1.5\pi$ for $L=4n$ and in $0<\phi<0.5\pi$ and $1.5\pi<\phi<2\pi$ for $L=4n+2$. Note that we find the similar first-order transitions at $K=K_{c1}$ mentioned previously in LDOS to also appear in PC for $L=4n+1$ and $L=4n+3$; while PC is continuous at $K=K_{c1}$ for $L=4n$ and $L=4n+2$. Despite the above differences, we find two common features in Fig. 11 that remain the same as in the case of $K=0$: (i) $I_N(\phi)=I_{N+2}(\phi+\pi)$ and (ii) PC for $L=$even is larger than that for $L=$odd.

2. Varies L with fixed K

Figures 12 and 13 show PC versus magnetic flux at different system sizes. In the following the discussion is separated into two cases: (i) $K<K_c$ [case (I)] where PC increases

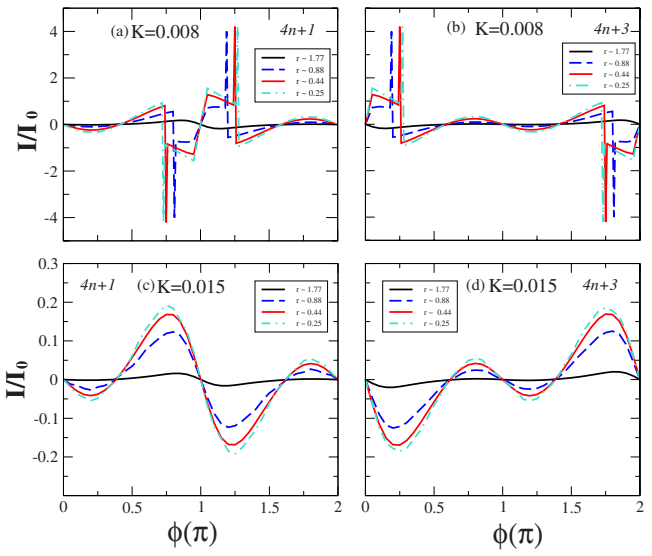

FIG. 12. (Color online) Persistent current with various L and fixed K (in unit of t). (a) $L=4n+1$, $K=0.008$; (b) $L=4n+3$, $K=0.008$; (c) $L=4n+1$, $K=0.015$; and (d) $L=4n+3$, $K=0.015$. Here, $r=\xi_k^0/L$. The parameters are: $\epsilon_d=-0.8t$, $t_R=t_L=0.4t$, and $\phi=0$. Here, we set $t=1$.

with increasing size L, and (ii) $K>K_c$ [case (II)] where PC decreases to 0 as L reaches the thermodynamic limit.

a. $K\leq K_c$. We first look at cases with $K<K_c$. Figure 12 shows PC versus magnetic flux with different size L for $K=0.008$ and $K=0.015$ (in unit of t). For $K=0.008$ [see Figs. 12(a) and 12(b)], as L is increased we find that PC exhibits two different behaviors: near $\phi=\pi$ for $L=4n+1$ and $\phi=0,2\pi$, for $L=4n+3$ PC changes from the behavior in crossover region to the Kondo state at $K=0$ [see Figs. 10(b) and 10(d)]; while out of these ranges of ϕ its behavior remains the same as in the crossover region but with an increasing amplitude. A first-order transition is seen to separate these two regions. We expect that at much larger system size the Kondo phase will be restored eventually over the entire range of ϕ. We have also investigated PC for $L=4n,4n+2$ (not shown here) and find the same qualitative behaviors except that instead of first-order transitions we find continuous changes in PC. Also, the behavior in $I_{4n+1}^{\phi\sim\pi}$ (or equivalently $I_{4n+3}^{\phi\sim 0}$) is the same as that for $K=0$ for all the sizes we investigate, suggesting that the Kondo phase is very easily restored in these ranges of ϕ.

On the other hand, for a larger value of $K=0.015$ [see Figs. 12(c) and 12(d)], as L increases from $L\sim 60$ to $L\sim 420$ (or $r=\xi_k^0/L$ changes from 1.77 to 0.25) PC still stays in the crossover region with an increasing amplitude. This is expected as for larger value of K one must go to much larger system size to observe the restoring of the Kondo effect in PC.

b. $K\geq K_c$. We now investigate the case where $K>K_c$. As shown in Fig. 13, since $K>K_c$ in this case, PC decreases in amplitude with increasing system size L and finally the system reaches the local spin-singlet state with vanishing PC. Note that $I_{4n}^{\phi\sim 0}$ and correspondingly $I_{4n+2}^{\phi\sim\pi}$ are always vanishingly small for all the sizes we investigate, suggesting the systems are already in the local spin-singlet states from the start for these ranges of ϕ, which is consistent with our mean-field phase diagram. However, for the remaining ranges of ϕ the systems start from the crossover region for smaller sizes and reach finally to the local spin-singlet state at large size.

From above results for PC, it implies that by applying magnetic flux, we may change the ground state of our system at finite sizes either from the local spin-singlet state to the crossover region or from the Kondo phase to the crossover region.

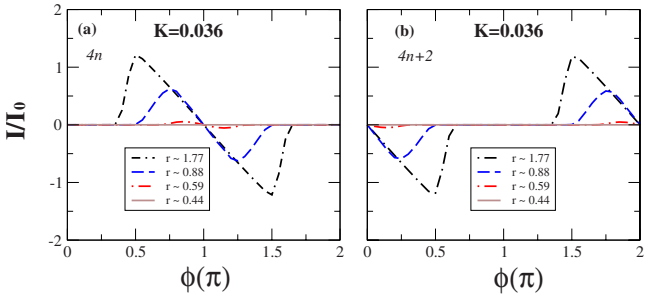

FIG. 13. (Color online) Persistent current with various L and fixed K. (a) $L=4n$. (b) $L=4n+2$. Here, $r=\xi_k^0/L$. Other parameters of data: $\epsilon_d=-0.8t$, $t_R=t_L=0.4t$, and $K=0.036$ (in unit of t). Here, we set $t=1$.

IV. DISCUSSIONS

We would like to make a few remarks on the validity of our mean-field approach and the qualitative behaviors of our results at finite sizes. First, we address the validity of our slave-boson mean-field approach to our problem. It is known that the slave-boson mean-field approach cannot correctly describe certain aspects of the antiferromagnetic exchange coupling due to the second-order hopping process. For example, the slave-boson approach to the t-J model in the context of high-T_c cuprates cannot correctly reproduce the antiferromagnetic long-range Néel order at zero doping. Nevertheless, if there are only two local spins coupled via antiferromagnetic exchange coupling, the $SU(N)$ mean-field theory can qualitatively capture the local (short-ranged) antiferromagnetic spin fluctuations when the system is close to the local spin-singlet Fermi-liquid ground state. In particular, a closely related side-coupled double quantum dot system by an antiferromagnetic RKKY coupling via a similar slave-boson mean-field approach has been recently studied in Ref. 11. The only difference between the setup in Ref. 11 and ours is the conduction-electron baths (leads)– two Fermi-liquid leads with continuous spectrum are considered in Ref. 11; while a finite-sized tight-binding ring is considered here. Compared to the more accurate numerical renormalization-group approach,[14] while the slave-boson mean-field approach in Ref. 11 cannot account for the crossover regime, $T^*<\omega<T_k/\ln(T_k/T^*)$, it correctly captures the Fermi-liquid regimes, $\omega\ll T^*$, and $T_k/\ln(T_k/T^*)<\omega<T_k$. In particular, the slave-boson mean-field approach in Ref. 11 correctly gives the crossover energy scale T^* and the form of LDOS $\rho_{QD}(\omega)$

on dot 1 which for $\omega < T^*$ shows symmetric double peaks with respect to $\omega=0$ and vanishes at $\omega=0$. As shown in Fig. 6, the crossover region that we focus on here is much less than T^*, $1/(T^*L) \ll 1$. Therefore, we expect that the slave-boson mean-field approach here is able to give a qualitatively correct description of the crossover region close to the two Fermi-liquid ground states, the Kondo, and the local spin-singlet phases.

Second, we try to explain the possible origin of the different finite-size crossover behaviors seen for $K \leq K_{c1}$ (at the mean-field level), a continuous transition for $L=4n$, a kinklike behavior for $L=4n+2$, and first-order transitions for $L=4n+1,4n+3$. We may explain these qualitatively different behaviors in terms of the different symmetries of the Kondo and local spin-singlet states which exhibit at finite sizes. In all four cases, the LDOS of the local spin-singlet phase has symmetric double peaks centered at $\omega=0$. The Kondo state at finite sizes, however, shows different symmetries depending on L: LDOS shows a main single symmetric Kondo peak at $\omega=0$ for $L=4n$, a single main Kondo peak for $\omega<0$ for $L=4n+1$, and a single main Kondo peak for $\omega>0$ for $L=4n+3$, and asymmetric double peaks around $\omega=0$ for $L=4n+2$.

At the mean-field level, crossover region can be regarded as the coexisting phase between Kondo and spin-singlet state. If the symmetries of the two states are the same, a continuous transition is expected at the boundary K_{c1} between the Kondo and the coexisting states. Case (I) ($L=4n$) belongs to this case. However, if the symmetries between the two are very different, a level-crossing-type first-order transition is expected at the boundary, such as for $L=4n+1$ and $4n+3$. For $L=4n+2$, the symmetries between Kondo and spin-singlet states are somewhat similar (both show double peaks in LDOS) but with a difference (the double peaks in LDOS for Kondo state are not symmetric with respect to $\omega=0$ while the double peaks in the local spin-singlet state are symmetric), which may explain the kinklike behavior at K_{c1} that we observe in our results.

V. CONCLUSIONS

To summarize, we have studied via large-N slave-boson mean-field approach the Kondo effect in a side-coupled double quantum dot system where one dot is embedded in a mesoscopic ring. The competition between the Kondo effect and the antiferromagnetic spin-spin interaction in this geometry gives rise to the Kosterlitz-Thouless quantum phase transition with at a finite value of $K=K_c$ in the thermodynamic limit. The mean-field phase diagrams of the model depends on the finite size L (mod 4): for $L=4n,4n+1,4n+3$ [case (I)] as K is increased, the crossover to the spin-singlet phase occurs at $K_{c2}<K_c$; while for $L=4n+2$ [case (II)] the crossover to the spin-singlet phase takes place at $K_{c2}>K_c$. To further study how the Kondo screening is suppressed by the RKKY coupling, we have performed a systematic finite-size analysis on the Kondo temperature T_k, the local density of states on the dot $\rho_{QD}(\omega)$ which connects to the ring, and the persistent current PC induced by the magnetic flux penetrating through the ring. For $L=4n$ with a fixed $K<K_c$, we find all the above quantities flow to the Kondo phase with a reduced Kondo temperature $T_k<T_k^0$ system size is increased: T_k and PC increase in magnitude and $\rho_{QD}(\omega)$ develops a pronounced single Kondo peak centered at $\omega=0$; while for $K>K_c$, the flows at finite sizes for $L=4n+2$ are toward the local spin-singlet phase with $T_k=0$ where all of the three observables decrease in magnitude to 0 with increasing size. From the finite-size scaling of T_k for $L=4n,4n+2$, we have shown that T_k is an universal function of $1/(LT^*)$ for $1/L<T^*$ where T^* has been unambiguously identified the characteristic Kosterlitz-Thouless crossover energy scale: $T^*=c\tilde{T}_k \exp[-\pi\tilde{T}_k/(K-K_c)]$. For $L=4n+1,4n+2,4n+3$, we find the ground state remains in the Kondo phase for $K<K_{c1}$ and it crossovers to the local spin-singlet phase for $K_{c1}<K<K_{c2}$ and finally reaches the spin-singlet phase for $K>K_{c2}$. For $L=4n+1,4n+3$, we find the first-order transitions in all of the three observables at the phase boundary between Kondo and the crossover regions, $K=K_{c1}$; while for $L=4n+2$ we find a "kinklike" behavior at $K=K_{c1}$. We believe these singular behaviors for $K \leq K_{c1}$ are due to artifacts of the large-N mean-field theory at finite sizes. Further finite-size analysis on T_k indicates that these singular behaviors for $L=4n+1,4n+2,4n+3$ are expected to vanish and the Kosterlitz-Thouless transition is expected to occur in the thermodynamic limit. In particular, for $L=4n+2$, we find for K being sufficiently close to K_c and for large system sizes the crossover still follows the same typical Kosterlitz-Thouless transition as that for $L=4n$. Note that unlike the similar system studied previously on the side-coupled double-dot system embedded in conduction-electron Fermi sea with constant density of states, the key finding in this paper is the KT transition with a finite value of $K_c>0$ in a side-coupled double-dot system embedded in a mesoscopic ring (in stead of $K_c=0$ for the system with Fermi sea of continuous spectrum). Whether this finite K_c is due to the artifact of the mean-field theory or due to the more singular density of states of the one-dimensional tight-binding ring needs further investigations. Our results on the transport properties of the system are relevant for future experiments on the side-coupled double quantum dot system embedded in a mesoscopic ring.

ACKNOWLEDGMENTS

We are grateful for the useful discussions with G. M. Zhang, C. S. Chu, J. J. Lin, J. C. Chen, and K. Le Hur. We also acknowledge the generous support from the NSC Grants No. 95-2112-M-009-049-MY3, No. 98-2918-I-009-006, No. 98-2112-M-009-010-MY3, the MOE-ATU program, the NCTS of Taiwan, R.O.C., and National Center for Theoretical Sciences (NCTS) of Taiwan.

[1] A. C. Hewson, *The Kondo Problem to Heavy Fermions* (Cambridge University Press, Cambridge, 1997).
[2] L. Kouwenhoven and L. Glazman, Phys. World **14**, 33 (2001).
[3] D. Goldharber-Gorden, H. Shtrikman, D. Mahalu, D. Abusch-Magder, U. Meirav, and M. A. Kastner, Nature (London) **391**, 156 (1998); S. M. Cronenwett, T. H. Oosterkamp, and L. P. Kouwenhoven, Science **281**, 540 (1998); For a review: D. Goldharber-Gorden, J. Göres, H. Shtrikman, D. Mahalua, U. Meirava, and M. A. Kastner, Mater. Sci. Eng., B **84**, 17 (2001).
[4] I. Affleck and P. Simon, Phys. Rev. Lett. **86**, 2854 (2001); P. Simon and I. Affleck, Phys. Rev. B **64**, 085308 (2001).
[5] H. Hu, G.-M. Zhang, and L. Yu, Phys. Rev. Lett. **86**, 5558 (2001).
[6] K. Kang and S.-C. Shin, Phys. Rev. Lett. **85**, 5619 (2000).
[7] K. G. Wilson, Rev. Mod. Phys. **47**, 773 (1975).
[8] N. J. Craig, J. M. Taylor, E. A. Lester, C. M. Marcus, M. P. Hanson, and A. C. Gossard, Science **304**, 565 (2004).
[9] G. Zaránd, C.-H. Chung, P. Simon, and M. Vojta, Phys. Rev. Lett. **97**, 166802 (2006).
[10] P. Simon, R. López, and Y. Oreg, Phys. Rev. Lett. **94**, 086602 (2005).
[11] P. S. Cornaglia and D. R. Grempel, Phys. Rev. B **71**, 075305 (2005).
[12] P. Simon, Phys. Rev. B **71**, 155319 (2005).
[13] B. A. Jones, C. M. Varma, and J. W. Wilkins, Phys. Rev. Lett. **61**, 125 (1988); B. A. Jones and C. M. Varma, Phys. Rev. B **40**, 324 (1989); I. Affleck, A. W. W. Ludwig, and B. A. Jones, *ibid.* **52**, 9528 (1995).
[14] C. H. Chung, G. Zaránd, and P. Wölfle, Phys. Rev. B **77**, 035120 (2008).
[15] L. G. G. V. Dias da Silva, N. Sandler, P. Simon, K. Ingersent, and S. E. Ulloa, Phys. Rev. Lett. **102**, 166806 (2009).
[16] M. Büttiker and C. A. Stafford, Phys. Rev. Lett. **76**, 495 (1996); Pascal Cedraschi, Vadim V. Ponomarenko, and Markus Büttiker, *ibid.* **84**, 346 (2000).
[17] J. B. Marston and I. Affleck, Phys. Rev. B **39**, 11538 (1989).
[18] V. Chandrasekhar, R. A. Webb, M. J. Brady, M. B. Ketchen, W. J. Gallagher, and A. Kleinsasser, Phys. Rev. Lett. **67**, 3578 (1991); W. Rabaud, L. Saminadayar, D. Mailly, K. Hasselbach, A. Benoît, and B. Etienne, *ibid.* **86**, 3124 (2001).